ANZIAM J. (First published online 2024), page 1 of 21*
doi:10.1017/S1446181124000221
*Provisional—final page numbers to be inserted when paper edition is published

EFFECT OF NONUNIFORM POROSITY IN CURVED BREAKWATER ON WATER WAVES

DIBAKAR MONDAL[1], ANUSHREE SAMANTA[2], GOUR DAS[3] and SUDESHNA BANERJEA[3]

(Received 5 March, 2024; accepted 19 July, 2024)

Abstract

Assuming linear theory, the phenomenon of scattering of waves by a circular arc shaped barrier with nonuniform porosity is studied. The water region is considered to be of infinite or finite depth. Based on a judicious application of Green's integral theorem, the corresponding boundary value problem is reduced to a hypersingular integral equation of second kind. The boundary element method and the collocation method are adopted to solve the hypersingular integral equation, and we ensure a good matching of the solutions obtained by the two methods. The reflection coefficient and energy dissipation are evaluated by using the solution of the integral equation which is then studied graphically. Different choices of distributions of pores on the barrier are considered, and we observe that the nonuniform porosity of the barrier has significant effect on the reflected wave and the energy dissipation.

2020 *Mathematics subject classification*: 76B.

Keywords and phrases: curved barrier, variable porosity, hypersingular integral equation, collocation method, boundary element method, reflection coefficient, transmission coefficient, energy dissipation.

1. Introduction

Breakwaters, also known as wave attenuators, are coastal structures built out into the sea to protect a coast or harbour from the force of waves. These are usually bottom founded rigid structures that are expensive to construct, particularly for deep water,

[1]Department of Mathematics, Government General Degree College at Kalna-I, Muragacha, Medgachi, Purba Burdwan 713405, India; e-mail: dibakar12.87@gmail.com
[2]Techno India University, EM block, Sector-V, Kolkata 700091, India;
e-mail: anushreesamanta14@gmail.com
[3]Department of Mathematics, Jadavpur University, Kolkata 700032, India;
e-mail: gourdas20132014@gmail.com, sudeshna.banerjea@yahoo.co.in

and these also prevent the natural water circulation, leading to environmental issues. Floating breakwaters are useful alternatives that are cost effective and have low impact on the environment. These types of breakwaters are usually kept floating by using a proper mooring system [2, 17]. Floating breakwaters can be of various shapes and configurations. A floating breakwater in the form of an arc of a circle encountering water waves is important, because it is known that the increase in arc length of a circular arc shaped rigid breakwater reduces the reflection of waves [12]; therefore, most of the wave energy can be utilized. This has an important bearing on the construction of a wave energy device. An important application of a circular arc shaped breakwater is as a semi-circular caisson whose major advantage is its stability against sliding [5]. As reported in [5], many experimentalists have studied the effect of waves on a circular arc shaped barrier for construction of coastal structures in the form of curved breakwaters and they verified the experimental result with a theoretical one.

The phenomenon of a wave encounter with a barrier in the form of a circular arc shaped rigid structure submerged in water under linear theory has been studied by many researchers using various mathematical tools. Notable among them are Parsons and Martin [12], McIver and Urka [7], Kanoria and Mandal [4], and Mondal et al. [11].

Recently, there has been a surge in the number of studies on porous breakwaters as the pores are dissipators of energy which reduce wave action and maintain water circulation. Wave propagation over a porous circular arc shaped barrier has been studied by many researchers like Liu and Li [5], Mondal et al. [8], Mondal and Banerjea [9], and Samanta et al. [13].

The study of a wave interaction with barriers with nonuniform porosity is limited in the literature, although studies in connection with the problem of a wave interaction with a perforated cylindrical breakwater with nonuniform porosity in the circumferential direction and uniform porosity in the vertical direction were initiated by Tao et al. [19] in 2009 using the eigenfunction expansion method. Song and Tao [18] in 2010 adopted an efficient numerical method to study water wave interaction with a cylinder with a nonuniform porosity, and their numerical experiments established the efficacy and accuracy of their numerical method. In these studies, the authors mention that two-dimensional studies on the interaction of ocean surface waves with a porous breakwater have limitations as in reality, the ocean waves are more complex and are better described by three-dimensional short-crested waves. They also found that by making the porosity nonuniform, the various features of wave motion become more complex than its counterpart of uniform porosity.

Recently, the problem related to wave interaction with dual porous barriers with nonuniform porosity was studied by Gupta and Gayen [3] and Sarkar et al. [15] using coupled integral equation formulation. Later, Singh et al. [16] studied the phenomenon of water wave propagation in the presence of an inclined flexible plate with variable porosity using hypersingular integral equation formulation. Mondal et al. [10] and Banerjee et al. [1] studied the effect of nonuniform porosity of a porous vertical barrier

https://doi.org/10.1017/S1446181124000221 Published online by Cambridge University Press

on an obliquely incident wave train by using Fredholm integral equation formulation. Banerjee et al. [1] showed that for a certain choice of porosity distribution, the wave energy dissipation by a barrier with nonuniform porosity is more than that of a barrier with uniform porosity. This choice of porosity distribution in a barrier with nonuniform porosity enhances its efficiency as a breakwater more than a barrier with uniform porosity.

In the present paper, we study the behaviour of water waves in the presence of a thin circular arc shaped porous barrier with variable porosity. Based on a judicious application of Green's integral theorem, the corresponding boundary value problem is reduced to a second kind of hypersingular integral equation.

The hypersingular integral equation is a powerful mathematical tool which is very useful in studying scattering problems involving barriers of different geometry. Usually, the problem of scattering by a rigid barrier can be formulated in terms of a first kind of hypersingular integral equation whereas the scattering problems involving porous barriers give rise to a second kind of hypersingular integral equation. Parsons and Martin [12] were pioneers in applying the collocation method to solve a hypersingular integral equation where they approximated the unknown function by Chebychev's polynomial. Samanta et al. [13] recently used the boundary element method to solve a hypersingular integral equation in a very simple manner. This is a useful alternative method of solution.

In the present study, following [11, 14], the second kind of hypersingular integral equation was solved by using the boundary element method as well as the collocation method. We may mention here that the kernel of the hypersingular integral equation in the case of finite depth is more complicated than that for infinite depth and, as such, the numerical solution of the hypersingular integral equation arising in the case of finite depth is more time consuming than its counterpart for infinite depth. So the solution of the integral equation in both cases is interesting from the mathematical and numerical points of view. Also, the collocation method converges faster than the boundary element method, but the advantage of the boundary element method is that it is very simple computationally, particularly when the kernel is complicated. The convergence of the boundary element method is discussed in detail in [13]. Using the solution of the hypersingular integral equation, the quantities of physical interest, namely, the reflection coefficient and amount of energy dissipated are determined in terms of the porosity distribution function. These physical quantities are then depicted graphically considering two types of porosity distributions in the barrier. It was observed that the reflection coefficients obtained by using the solution of the hypersingular integral equation by the two methods are in good agreement up to a desired degree of accuracy. In the present study, we have chosen the distribution of nonuniform porosity in the barrier as a linear function and also as a quadratic function of the parameter which varies along the arc length of the curved barrier. The physical quantities like reflection and transmission coefficients and energy dissipation are evaluated for these two types of chosen porosity distributions. Other types of distributions of porosity may be considered for which the physical quantities of interest can be evaluated

https://doi.org/10.1017/S1446181124000221 Published online by Cambridge University Press

from the present method. The advantage of a nonuniform porosity distribution in the barrier over uniform porosity distribution is that a proper choice of nonuniform porosity distribution in the barrier can enhance the wave energy dissipation more than a barrier with uniform porosity. This is useful in the reduction of wave power and thereby protects the coastal region from the effect of the rough sea. This is illustrated graphically for a particular choice of porosity distribution in the barrier. We mention here that the results concerning the physical quantities of interest, namely, reflection coefficient, transmission coefficient and energy dissipation for deep water, can be recovered from the results of the finite depth case by making the water depth large. However, it is not easy to reduce the hypersingular integral equation for finite depth to that for the infinite depth case by making the water depth tend to infinity. Thus, it is interesting to study mathematically the hypersingular integral equation both for deep water and for water of finite depth. In the present study, we recover the numerical results for the reflection coefficient for deep water from the results for finite depth by making the depth very large.

2. Problem formulation

Under the assumption of linearized theory, we study a two-dimensional irrotational motion in water due to scattering of a normally incident wave train by a thin porous circular arc shaped barrier submerged in water. A rectangular Cartesian coordinate system is chosen where the y-axis is taken vertically downwards into the fluid and the x-axis is along the undisturbed free surface. A two-dimensional motion is justified due to the reason that motion in every cross section $z = c, c$ being an arbitrary constant, is similar [6]. Here, we study the motion for two cases when the water region is infinitely deep and also when water is of finite depth H. The water occupies the region $-\infty < x < \infty;\ 0 < y < \infty$ for deep water (DW) and the region $-\infty < x < \infty;\ 0 < y < H$ when the depth of water is finite (FDW). The circular arc shaped barrier C of radius u is placed symmetrically about the y-axis, with centre at $(0, v + u)$, and the radius through end points makes an angle θ with the y-axis. A schematic diagram of the problem is given by Figure 1.

For a train of time harmonic surface waves from negative infinity, with circular frequency σ represented by $Re\{\phi^{inc}(x, y)e^{-i\sigma\tau}\}$, when incident on the porous thin circular arc shaped barrier C, a part of it is reflected, and a part is transmitted above and below the barrier, as shown in Figure 1.

The resulting motion is described by the velocity potential $Re\{\phi(x, y)e^{-i\sigma\tau}\}$, where $\phi(x, y)$ satisfies the following boundary value problem:

$$\begin{aligned} &\nabla^2\phi = 0 \quad \text{in the fluid region,} \\ &K\phi + \phi_y = 0 \quad \text{on } y = 0, \\ &r^{1/2}\nabla\phi \quad \text{is bounded as } r \to 0, \end{aligned} \tag{2.1}$$

https://doi.org/10.1017/S1446181124000221 Published online by Cambridge University Press

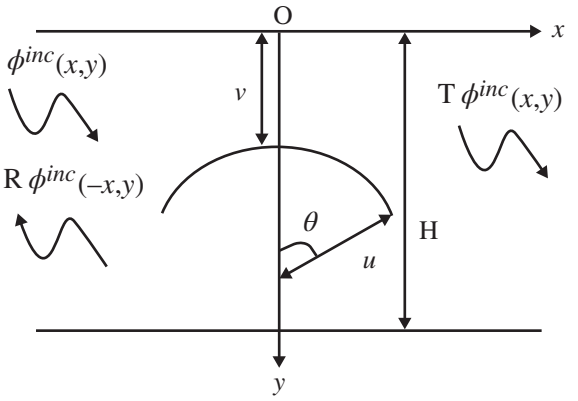

FIGURE 1. Schematic diagram of the problem.

where r is the distance of any point in the fluid region from either of the sharp ends of the barrier and

$$\nabla\phi \to 0 \quad \text{as } y \to \infty \text{ for DW},$$
$$\frac{\partial\phi}{\partial y} = 0 \quad \text{on } y = H \text{ for FDW}.$$

The boundary condition on the curved plate surface C is given by

$$\frac{\partial\phi(q+)}{\partial n} = \frac{\partial\phi(q-)}{\partial n} = -i\kappa\lambda(q)\,[\phi](q) \quad \text{on } C, \tag{2.2}$$

where

$$\kappa = \begin{cases} K = \sigma^2/g & \text{for DW}, \\ k_0 & \text{for FDW}, \end{cases}$$

and k_0 is the unique real positive root of the transcendental equation $k\tanh(kH) = K$.

Here, $[\phi](q) = \phi(q+) - \phi(q-)$ $(q \in C)$ is the difference of the potential function across the curved barrier C, where

$$q+ = \{(x,y) \in C \mid x^2 + (y - v - u)^2 > u^2\},$$
$$q- = \{(x,y) \in C \mid x^2 + (y - v - u)^2 < u^2\},$$

$\partial/\partial n$ denotes the normal derivative at a point on C, and $\lambda(q) = \lambda_r(q) + i\lambda_i(q)$ represents the nonuniform porosity parameter [16] which varies along the arc length of the barrier C. Here, $\lambda_r(q)$ denotes the resistance force coefficient and $\lambda_i(q)$ denotes the inertial force coefficient of the porous barrier, and if $\lambda_r >> \lambda_i$, then λ is taken to be real. Note that the resistance force coefficient $\lambda_r(q)$ resists the passage of water through the pores, while the inertial force coefficient $\lambda_i(q)$ allows the flow of water through the pores [20].

https://doi.org/10.1017/S1446181124000221 Published online by Cambridge University Press

The far-field condition is

$$\phi(x,y) \sim \begin{cases} \phi^{inc}(x,y) + R\phi^{inc}(-x,y) & \text{as } x \to -\infty, \\ T\phi^{inc}(x,y) & \text{as } x \to \infty, \end{cases} \tag{2.3}$$

where R and T are the reflection and transmission coefficients, respectively, which are to be determined. Here, the barrier C is represented parametrically as

$$C: \ x = u\sin s\theta; \ y = v + u - u\cos s\theta; \ -1 \le s \le 1; \ -\pi < \theta < \pi$$

and

$$\phi^{inc}(x,y) = g(y)e^{i\kappa x},$$

where

$$g(y) = \begin{cases} e^{-Ky} & \text{for DW}, \\ \dfrac{\cosh k_0(H-y)}{\cosh k_0 H} & \text{for FDW}. \end{cases}$$

3. Method of solution

Let $G(x,y;\xi,\eta)$ be the Green's function which is the velocity potential due to the presence of a line source at (ξ,η) in the fluid region whose expressions are given below [6].

For DW,

$$G(x,y;\xi,\eta) = \log\left(\frac{r_-}{r_+}\right) - 2\int_0^\infty \frac{e^{-k(y+\eta)}}{k-K}\cos k(x-\xi)\,dk. \tag{3.1}$$

For FDW,

$$G(x,y;\xi,\eta) = \log\left(\frac{r_-}{r_+}\right) - 2\int_0^\infty \left[\frac{\cosh k(H-y)\cosh k(H-\eta)}{k\sinh kH - K\cosh kH} + \frac{e^{-kH}\sinh k\eta \sinh ky}{k}\right]\frac{\cos k(x-\xi)}{\cosh kH}\,dk, \tag{3.2}$$

where $r_\mp = \sqrt{(x-\xi)^2 + (y\mp\eta)^2}$, and the infinite integrals in (3.1) and (3.2) can be evaluated by standard procedure [12].

We apply the Green's integral theorem to the scattered potential $(\phi - \phi^{inc})(x,y)$ and the source potential $G(x,y;\xi,\eta)$ on the region (as shown in Figure 2), bounded externally by the lines $y = 0, -X_1 \le x \le X_1$; $x = -X_1, 0 \le y \le Y_1$; $y = Y_1, \ -X_1 \le x \le X_1$; $x = X_1, 0 \le y \le Y_1$; and internally by a very small circle of radius δ centring (ξ,η) and a contour enclosing curve barrier C. It may be noted that for FDW, $Y_1 = H$ and for DW, Y_1 will tend to infinity. Making $X_1 \to \infty$, $\delta \to 0$ and $Y_1 \to \infty$

https://doi.org/10.1017/S1446181124000221 Published online by Cambridge University Press

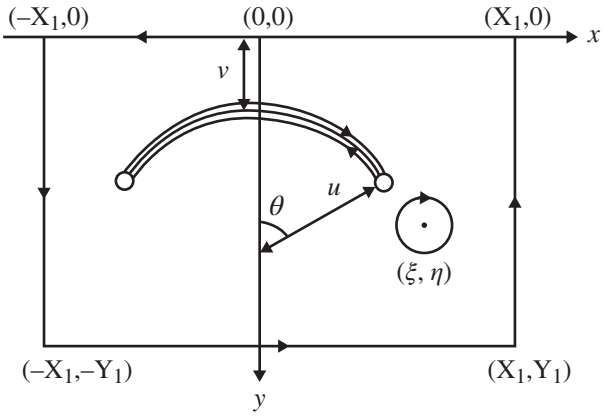

FIGURE 2. Contour for Green's integral theorem.

for DW and $Y_1 \to H$ for FDW, respectively, a representation of the potential function in terms of the unknown function $[\phi(p)]$ is obtained as

$$\phi(q) = \phi^{inc}(q) - \frac{1}{2\pi}\int_C [\phi](p)\frac{\partial}{\partial n_p}G(p,q)\,ds_p. \tag{3.3}$$

In obtaining the above representation, we have used (2.1) and the fact that $\nabla^2 G = 0$ except at (ξ,η). Also note that the line integrals over all outer boundaries are zero because of the fact that both $(\phi - \phi^{inc})(x,y)$ and G satisfy similar boundary conditions on all the outer boundaries. The only contribution comes from the contour C enclosing the barrier and the small circle of radius δ enclosing the point (ξ,η) (Figure 2 and [6]). In (3.3), $q = (\xi,\eta)$ is a field point, $p \equiv (x,y)$ is a point on barrier C, $[\phi](p)$ is the discontinuity of potential function $\phi(x,y)$ across C and $\partial/\partial n_p$ is the normal derivative at the point p on C. It may be noted that the unknown function $[\phi](p)$ vanishes at the end points of the arc-shaped barrier [6].

Using the boundary condition (2.2) on the barrier in (3.3), we obtain the following second kind of hypersingular integral equation:

$$\frac{1}{2\pi}\,\text{⨍}\!\!\!\!\!\!-\int_C [\phi](p)\frac{\partial^2}{\partial n_q \partial n_p}G(p,q)\,ds_p \;-\; i\kappa\,\lambda(q)\,[\phi](q) \;=\; \frac{\partial \phi^{inc}}{\partial n_q}(q), \quad q \in C, \tag{3.4}$$

where $\partial/\partial n_q$ is the normal derivative at the point q on C. The parametric equation of C at the points $p = (x,y)$ and $q = (\xi,\eta)$ in (3.4) is given by

$$\begin{aligned} x(s) &= u\sin s\theta, \quad y(s) = v + u - u\cos s\theta; \quad -1 \le s \le 1,\\ \xi(t) &= u\sin t\theta, \quad \eta(t) = v + u - u\cos t\theta; \quad -1 \le t \le 1. \end{aligned} \tag{3.5}$$

Thus, with the help of the parametrization given by (3.5) along with the introduction of a new unknown function $f(s) = [\phi](p(s))$, the integral equation (3.4) can be rewritten as

https://doi.org/10.1017/S1446181124000221 Published online by Cambridge University Press

$$\int_{-1}^{1} f(s)\left[\frac{1}{(s-t)^2} + u^2\theta^2\mathcal{L}(s,t)\right]ds + 2\pi i u\theta\kappa\lambda(t)f(t) = 2\pi u\theta g_1(t), \tag{3.6}$$

where

$$g_1(t) = \begin{cases} Ke^{-K\eta(t)+i(K\xi(t)+t\theta)} & \text{for DW,} \\ \dfrac{k_0 e^{ik_0\xi(t)}\sinh\left(k_0(H-\eta(t))+\imath t\theta\right)}{\cosh k_0 H} & \text{for FDW.} \end{cases}$$

The expression of $\mathcal{L}(s,t)$ is given as follows.

For DW,

$$\begin{aligned}\mathcal{L}(s,t) = &\left[\frac{1}{4u^2\sin^2((s-t)\theta/2)} - \frac{1}{u^2\theta^2(s-t)^2}\right] \\ &+ \cos(s-t)\theta\left[\frac{Y^2-X^2}{(X^2+Y^2)^2} + \frac{2KY}{X^2+Y^2} + 2K^2\Phi_0(X,Y)\right] \\ &+ 2\sin(s-t)\theta\left[K\frac{\partial\Phi_0}{\partial X} - \frac{XY}{(X^2+Y^2)^2}\right]\end{aligned}$$

with

$$X = x-\xi = u(\sin s\theta - \sin t\theta); \quad Y = y+\eta = 2v+2u-u(\cos s\theta+\cos t\theta),$$

$$\Phi_0(X,Y) = \imath\pi e^{-KY+\imath K|X|} + \int_0^\infty \frac{e^{-k|X|}}{k^2+K^2}\{k\cos kY - K\sin kY\}\,dk.$$

For FDW,

$$\begin{aligned}\mathcal{L}(s,t) = &\left[\frac{1}{4u^2\sin^2((s-t)\theta/2)} - \frac{1}{u^2\theta^2(s-t)^2}\right] \\ &+ \frac{X^2-Y^2}{(X^2+Y^2)^2}\cos(s-t)\theta - \frac{2XY}{(X^2+Y^2)^2}\sin(t-s)\theta \\ &+ 2\sin t\theta\sin s\theta\int_0^\infty \mu(k)\sinh k\eta\sinh ky\cos kX\,dk \\ &- 2\sin t\theta\cos s\theta\int_0^\infty \mu(k)\sinh k\eta\cosh ky\sin kX\,dk \\ &+ 2\cos t\theta\sin s\theta\int_0^\infty \mu(k)\cosh k\eta\sinh ky\sin kX\,dk \\ &+ 2\cos t\theta\cos s\theta\int_0^\infty \mu(k)\cosh k\eta\cosh ky\cos kX\,dk \\ &+ \sin t\theta\sin s\theta\Big[\zeta i\cosh k_0(H-y)\cosh k_0(H-\eta)\,e^{ik_0|X|} \\ &- \sum_{n=1}^{\infty}\omega_n\cos k_n(H-y)\cos k_n(H-\eta)\,e^{-k_n|X|} + \frac{2\pi}{H}\sum_{n=0}^{\infty}\alpha_n\sin\alpha_n y\sin\alpha_n\eta\,e^{-\alpha_n|X|}\Big]\end{aligned}$$

https://doi.org/10.1017/S1446181124000221 Published online by Cambridge University Press

$$+\cos t\theta\cos s\theta\Big[\zeta i\sinh k_0(H-y)\sinh k_0(H-\eta)\,e^{ik_0|X|}$$
$$+\sum_{n=1}^{\infty}\omega_n\sin k_n(H-y)\sin k_n(H-\eta)\,e^{-k_n|X|}-\frac{2\pi}{H}\sum_{n=0}^{\infty}\alpha_n\cos\alpha_n y\cos\alpha_n\eta\,e^{-\alpha_n|X|}\Big]$$
$$+\sin t\theta\cos s\theta\Big[\zeta\sinh k_0(H-y)\cosh k_0(H-\eta)\,e^{ik_0|X|}$$
$$-\sum_{n=1}^{\infty}\omega_n\sin k_n(H-y)\cos k_n(H-\eta)\,e^{-k_n|X|}+\frac{2\pi}{H}\sum_{n=0}^{\infty}\alpha_n\cos\alpha_n y\sin\alpha_n\eta\,e^{-\alpha_n|X|}\Big]$$
$$-\cos t\theta\sin s\theta\Big[\zeta\cosh k_0(H-y)\sinh k_0(H-\eta)\,e^{ik_0|X|}$$
$$-\sum_{n=1}^{\infty}\omega_n\cos k_n(H-y)\sin k_n(H-\eta)\,e^{-k_n|X|}+\frac{2\pi}{H}\sum_{n=0}^{\infty}\alpha_n\sin\alpha_n y\cos\alpha_n\eta\,e^{-\alpha_n|X|}\Big],$$

where k_0 and ik_n are roots of the transcendental equations $k\tanh kH-K=0$; $i\alpha_n$ terms are roots of the equation $\cosh kH=0$ and

$$\mu(k)=\frac{k\,e^{-kH}}{\cosh kH},\quad \zeta=\frac{4\pi k_0^2}{2k_0H+\sinh(2k_0H)},\quad \omega_n=\frac{4\pi k_n^2}{2k_nH+\sin(2k_nH)}.$$

It may be noted here that if $\lambda(t)=0$, then the hypersingular integral equation of second kind (3.6) reduces to a hypersingular integral equation of first kind. Also for $\lambda(t)=0$, the condition (2.2) on the porous barrier reduces to the condition on a rigid barrier. This shows that wave interaction with porous barrier produces the second kind of hypersingular integral equation, while that with a rigid barrier produces the first kind of hypersingular integral equation. It is also interesting to observe that the kernel of the hypersingular integral equation for water of finite depth is quite complicated in comparison to the kernel in the case of deep water.

The unknown physical quantities R and T are evaluated by making $\xi\to\mp\infty$ in (3.3) and comparing with the far-field condition for $\phi(\xi,\eta)$ as given by (2.3). This yields

$$R=\begin{cases}-iKu\theta\displaystyle\int_{-1}^{1}f(s)e^{-Ky(s)+iKx(s)s\theta}\,ds & \text{for DW,}\\ -\dfrac{2u\theta ik_0\cosh k_0H}{2k_0H+\sinh 2k_0H}\displaystyle\int_{-1}^{1}f(s)\sinh(k_0(H-y(s))+is\theta)\,e^{ik_0x(s)}\,ds & \text{for FDW,}\end{cases}\tag{3.7}$$

and

$$T=\begin{cases}1-iKu\theta\displaystyle\int_{-1}^{1}f(s)e^{-Ky(s)-iKx(s)s\theta}\,ds & \text{for DW,}\\ 1-\dfrac{2u\theta ik_0\cosh k_0H}{2k_0H+\sinh 2k_0H}\displaystyle\int_{-1}^{1}f(s)\sinh(k_0(H-y(s))-is\theta)\,e^{-ik_0x(s)}\,ds & \text{for FDW.}\end{cases}\tag{3.8}$$

https://doi.org/10.1017/S1446181124000221 Published online by Cambridge University Press

Thus, from (3.7) and (3.8), we observe that R and T are expressed in terms of the unknown function $f(s)$ which can be obtained by solving the integral equation (3.6).

3.1. Solution of the integral equation This section illustrates the boundary element method and the collocation method of the solution of the second kind of hypersingular integral equation (3.6). We may mention here that the numerical solution of the hypersingular integral equation is limited in the literature due to the reason that hypersingular integrals are not amenable to the numerical methods. Application of the collocation method using Chebychev's polynomial in solving the hypersingular integral equation was initiated by Parsons and Martin [12]. Later, Samanta et al. [13] applied the boundary element method to solve the hypersingular integral equation. The boundary element method is a simple method computationally, but the convergence of the collocation method is faster than the boundary element method. The present analysis demonstrates the application of two methods.

Boundary element method. We will solve the integral equation (3.6) numerically using the boundary element method (BEM). The method of solution of the hypersingular integral equation using BEM and the convergence study is described in detail in [13].

Since $[\phi] = 0$ at the ends of the barrier, we have $f(s) = 0$ at $s = \pm 1$. This behaviour asserts that we may assume

$$f(s) = \sqrt{1 - s^2}\psi(s), \tag{3.9}$$

where $\psi(s)$ is a regular function in $[-1, 1]$. Noting (3.9), the hypersingular equation (3.6) takes the form

$$\int_{-1}^{1} \sqrt{1 - s^2}\left[\frac{1}{(s - t)^2} + u^2\theta^2\mathcal{L}(s, t)\right]\psi(s)\, ds + 2\pi i u\theta\kappa\lambda(t)\sqrt{1 - t^2}\psi(t) = 2\pi u\theta g_1(t), \quad -1 \le t \le 1. \tag{3.10}$$

As per the BEM, the range of integration $[-1, 1]$ is divided into m number of equal line elements, that is, $[-1, 1] = \bigcup_{j=1}^{m}[a_{j-1}, a_j]$, where a_{j-1} and a_j are the end points of the jth line element, and $a_0 = -1$, $a_m = 1$ and $a_j = a_0 + jr'$, $r' = (a_m - a_0)/m$. Writing $s = s_j$ where $s_j \in [a_{j-1}, a_j]$, and $t = t_i$ where $t_i \in [a_{i-1}, a_i]$, $i, j = 1, 2, \ldots, m$,

$$s_j = (1 - \tau)a_{j-1} + \tau a_j, \quad 0 \le \tau \le 1; \quad t = t_i = (1 - \gamma)a_{i-1} + \gamma a_i, \quad 0 \le \gamma \le 1.$$

Thus, (3.10) takes the form

$$\sum_{j=1}^{m}\int_{0}^{1} \sqrt{1 - s_j^2}\left\{\frac{1}{(s_j - t_i)^2} + u^2\theta^2\mathcal{L}(s_j, t_i)\right\}\psi(s_j)\, r'\, d\tau + 2\pi i u\theta\kappa\lambda(t_i)\sqrt{1 - t_i^2}\psi(t_i) = 2\pi u\theta g_1(t_i), \quad i = 1, 2, \ldots, m. \tag{3.11}$$

https://doi.org/10.1017/S1446181124000221 Published online by Cambridge University Press

Assuming that the unknown function $\psi(s_j) = \psi_j$ is a constant for the jth line element, $j = 1, 2, \ldots, m$, the integral equation (3.11) is reduced to the following system of linear algebraic equations [14]:

$$\sum_{j=1}^{m} a_{ij}\, \psi_j = 2\pi u\theta g_{1i}, \quad i = 1, 2, \ldots, m, \tag{3.12}$$

where

$$a_{ij} = \int_0^1 \sqrt{1 - s_j^2}\left\{\frac{1}{(s_j - t_i)^2} + u^2\theta^2 \mathcal{L}(s_j, t_i)\right\} r'\, d\tau \; + \delta_{ij} 2\pi i u\theta\kappa\lambda(t_i)\sqrt{1 - t_i^2},$$
$$i = 1, 2, \ldots, m, \quad j = 1, 2, \ldots, m,$$
$$g_{1i} = g_1(t_i), \quad i = 1, 2, \ldots, m.$$

Now solving the system of linear equations (3.12), we obtain the unknown coefficients ψ_j, $j = 1, 2, \ldots, m$, and then we approximate the solution of $f(s)$ in each line interval to evaluate the value of R and T from (3.7) and (3.8).

Collocation method. In this method, the unknown function $f(s)$ is approximated as [12]

$$f(s) \approx \sqrt{1 - s^2} \sum_{n=0}^{N} d_n U_n(s), \tag{3.13}$$

where N is an integer, $U_n(s)$ is the nth-order Chebyshev polynomial of second kind, and d_n are unknown complex constants for each $n = 0, 1, 2, \ldots, N$.

Substituting $f(s)$ from (3.13) into hypersingular integral equation (3.6), we obtain the following system of algebraic equations [12]:

$$\sum_{n=0}^{N} d_n\, B_n(t) \; = 2\pi u\theta g_1(t), \quad -1 \le t \le 1, \tag{3.14}$$

where

$$B_n(t) = -\,\pi(n+1)U_n(t) \; + \; u^2\theta^2 \int_{-1}^{1} \sqrt{1 - s^2}\; U_n(s)\; \mathcal{L}(s, t)\, ds$$
$$+\, 2\pi i u\theta\kappa\lambda(t)\sqrt{1 - t^2}\; U_n(t).$$

The collocation points $t = t_j$ can be taken as

$$t_j = \cos\left(\frac{2j+1}{2N+2}\right)\pi, \quad j = 0, 1, 2, \ldots, N,$$

so that (3.14) yields the following system of linear equations:

$$\sum_{n=0}^{N} d_n\, B_n(t_j) \; = 2\pi u\theta\; g_1(t_j), \quad j = 0, 1, 2, \ldots, N, \tag{3.15}$$

https://doi.org/10.1017/S1446181124000221 Published online by Cambridge University Press

where d_n terms are unknown constants to be determined. Now we can approximate the solution $f(s)$ of the integral equation (3.6) by substituting d_n terms in (3.13), and then using it in (3.7) and (3.8), we can evaluate the value of reflection coefficient R and transmission coefficient T, respectively.

3.2. Energy identity The energy dissipation due to porosity yields $|R|^2 + |T|^2 < 1$, and this can be mathematically justified by applying Green's integral theorem to the functions ϕ and $\bar{\phi}$ in the suitable chosen region which results in the energy identity as

$$|R|^2 + |T|^2 = 1 - J,$$

where

$$J = \begin{cases} 2Ku\theta \displaystyle\int_{-1}^{1} |f(t)|^2 \, \lambda_r(t)\, dt & \text{for DW,} \\ \dfrac{2Ku\theta \cosh k_0 H}{k_0 H + (1/2)\sinh 2k_0 H} \displaystyle\int_{-1}^{1} |f(t)|^2 \, \lambda_r(t)\, dt & \text{for FDW} \end{cases} \tag{3.16}$$

is the energy dissipation coefficient.

4. Numerical results

In this section, the numerical estimates for reflection coefficients $|R|$ and energy dissipation coefficients J are studied graphically for deep water as well as finite depth of water. For DW, $|R|$ and J are depicted graphically against the dimensionless wave number Ku for different values of nondimensional parameters $v/u, \theta, \lambda(t)$. When the water region is of finite depth H (FDW), $|R|$ and J are plotted graphically against the wave number KH for different values of nondimensional parameters $v/H,\ u/H, \theta, \lambda(t)$.

The porosity parameter $\lambda(t) = \lambda_r(t) + i\lambda_i(t), -1 \le t \le 1$, is chosen here as:

(i) $\lambda(t) = (1 + t)/2$;
(ii) $(1 + i/2)(1 + t)/2$;
(iii) $\lambda(t) = t^2$;
(iv) $t^2(1 + i/2), \quad 1 \le t \le 1$.

We may mention here that when the inertial force coefficient is negligible as compared with the resistance force coefficient, then $\lambda(t)$ is taken to be real. The distribution of pores in each of the cases is described below.

(a) When $\lambda(t) = (1 + t)/2$, then $\lambda_i(t) = 0$ and $\lambda_r(t) = (1 + t)/2$, so that $\lambda(t) = \lambda_r(t)$ is real. In this case, the distribution of pores in the barrier is such that $\lambda(t) = 0$ for $t = -1$, that is, at one end of the barrier, and increases as t increases till $\lambda_r(t)$ reaches maximum value $\lambda_r(t) = 1$ at $t = 1$ (Figure 3(a)).

(b) When $\lambda(t) = (1 + i/2)(1 + t)/2$, then $\lambda_r(t) = (1 + t)/2$ and $\lambda_i(t) = (1 + t)/4$. In this case, at $t = -1$, $\lambda_r(t) = \lambda_i(t) = 0$, that is, at one end of the plate, porosity is zero. As t increases, $\lambda_r(t)$ and $\lambda_i(t)$ increase and reach maximum values $\lambda_r(t) = 1$ and $\lambda_i(t) = 1/2$, respectively. So $\lambda(t) = (1 + i/2)(1 + t)/2$ suggests that the distribution of pores in the barrier is such that the barrier is rigid at one end, and the porosity increases

https://doi.org/10.1017/S1446181124000221 Published online by Cambridge University Press

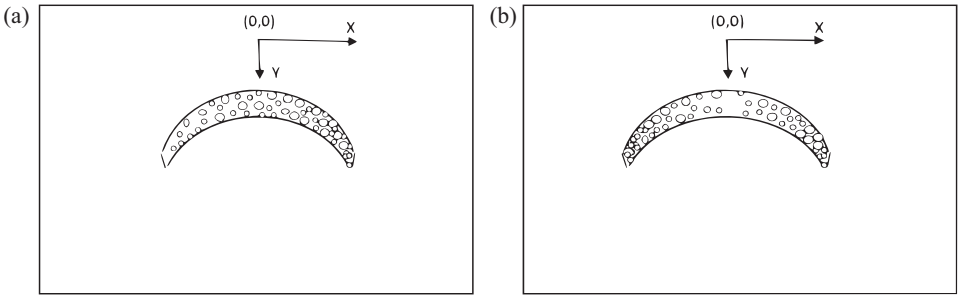

FIGURE 3. Porosity distribution of curved barrier (a) $\lambda(t) = (1 + t)/2$, (b) $\lambda(t) = t^2$.

TABLE 1. Reflection coefficient for $\theta = \pi/10$, $v/u = 0.1$, $\lambda(t) = t^2$.

Ku	BEM	Collocation method
0.5	0.110823	0.110881
1.0	0.393708	0.393773
1.5	0.585003	0.585089
2.0	0.628177	0.628244

along the barrier in the sense that the resistance force coefficient $\lambda_r(t)$ and inertial force coefficient $\lambda_i(t)$ increase linearly along the barrier, until at the other end, the resistance force coefficient and the inertial force coefficient reach a maximum value. Similarly, the distribution of pores in the barrier for $\lambda(t) = t^2, t^2(1 + i/2)$ is such that $\lambda(t) = 0$ for $t = 0$, that is, the barrier is rigid at the centre. The resistance force coefficient $\lambda_r(t)$ and inertial force coefficient $\lambda_i(t)$ increase towards the two ends of the barrier until they reach maximum values at $t = \pm 1$, that is, at the two ends of the barrier (Figure 3(b)).

The reflection coefficient $|R|$ and the amount of wave energy dissipated J can be computed numerically from (3.7) and (3.16), respectively, by solving the integral equation (3.6). For numerical computation, the value of m (number of elements) in (3.12) is chosen as $m = 45$ and the value of N (number of collocation points) in (3.15) is taken as 15. We may say here that the convergence of the collocation method is faster than BEM, but computation execution of BEM is simpler than the collocation method.

Tables 1 and 2 show a comparison of the values of $|R|$ obtained from BEM and the collocation method for DW with

$$Ku = \{0.5, 1.0, 1.5, 2.0\}, \quad \theta = \pi/10, \quad v/u = 0.1, \quad \text{for } \lambda(t) = \{t^2, t^2(1 + i/2)\}.$$

Similar comparisons of $|R|$ are presented in Tables 3 and 4 for FDW with

$$KH = \{0.5, 1.0, 1.5, 2.0\}, \theta = \pi/10, \ v/H = 0.3, \ u/H = 0.5,$$
$$\text{for } \lambda(t) = \{t^2, t^2(1 + i/2)\}.$$

https://doi.org/10.1017/S1446181124000221 Published online by Cambridge University Press

TABLE 2. Reflection coefficient for $\theta = \pi/10$, $v/u = 0.1$, $\lambda(t) = t^2(1 + i/2)$.

Ku	BEM	Collocation method
0.5	0.106467	0.106530
1.0	0.368472	0.368526
1.5	0.554586	0.554646
2.0	0.606203	0.606259

TABLE 3. Reflection coefficient for $\theta = \pi/10$, $v/H = 0.3$, $u/H = 0.5$, $\lambda(t) = t^2$.

KH	BEM	Collocation method
0.5	0.0065013	0.00655601
1.0	0.0213352	0.0213885
1.5	0.0412981	0.0413128
2.0	0.0603015	0.0603288

TABLE 4. Reflection coefficient for $\theta = \pi/10$, $v/H = 0.3$, $u/H = 0.5$, $\lambda(t) = t^2(1 + i/2)$.

KH	BEM	Collocation method
0.5	0.0064481	0.00647615
1.0	0.0208257	0.0208765
1.5	0.0393671	0.0398722
2.0	0.0573542	0.0576478

It is observed from Tables 1, 2, 3 and 4 that values of $|R|$ agree with each other up to 3 or 4 decimal places. The accuracy can be improved by increasing the number of line elements in the boundary element method and the number of collocation points N in the collocation method. Here, note that the energy identity, $|R|^2 + |T|^2 = 1$, has been verified for the rigid curve barrier, that is, $\lambda = 0$. Also, the energy identity $|R|^2 + |T|^2 + J = 1$ for a porous curve barrier has been verified.

The reflection coefficient $|R|$ for a rigid barrier, that is, for $\lambda = 0$ in deep water, is compared with the results of Parsons and Martin [12] in Figure 4(a) and in Figure 4(b), $|R|$ for rigid barrier, that is, for $\lambda = 0$ in finite depth water are compared with [5, Table 1]. It is observed that both results are in good agreement with each other. In Figure 5, $|R|$ for deep water is compared with $|R|$ for water of finite depth, for large depth, that is, $H/u = 3$, $v/u = 0.1$, $\theta = \pi/10$. A good matching of $|R|$ is observed for both infinite and finite depth of water region.

Behaviour of $|R|$ and J for deep water. In Figures 6(a)–6(c) and 7(a)–7(c), the reflection coefficient $|R|$ and the wave energy dissipation coefficient J are computed

https://doi.org/10.1017/S1446181124000221 Published online by Cambridge University Press

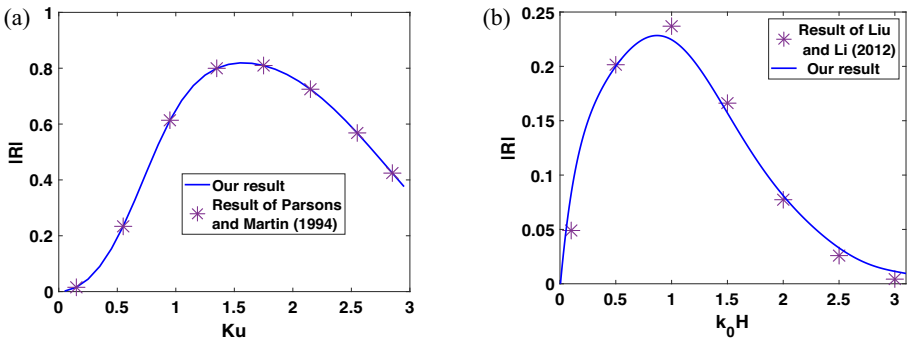

FIGURE 4. (a) Comparison between our result and the results of Parsons and Martin [12] for $v/u = 0.1$, $\theta = \pi/2$. (b) Comparison between our result and the results of Liu and Li [5] for $v/H = 0.5, u/H = 0.5$ and $\theta = \pi/2$.

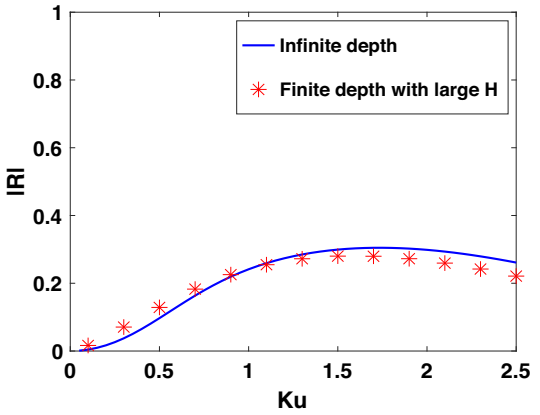

FIGURE 5. $|R|$ against Ku for deep water and for water of finite depth where $v/u = 0.1$, $\theta = \pi/10$, $H/u = 3$.

numerically for a barrier in deep water (DW) and depicted graphically against the wave number Ku, for $v/u = 0.1$, the porosity parameter $\lambda(t) = \{1, 1 + i/2, (1 + t)/2, (1 + i/2)(1 + t)/2, t^2, t^2(1 + i/2)\}$ and $\theta = \{\pi/10, 3\pi/10, \pi/2\}$. In Figures 8(a)–8(c) and 9(a)–9(c), the reflection coefficient $|R|$ and the wave energy dissipation coefficient J are computed numerically for a barrier in water of finite depth (FDW), and depicted graphically against the wave number KH, for $v/H = 0.3, u/H = 0.5$, the porosity parameter $\lambda(t) = \{1, 1 + i/2, (1 + t)/2, (1 + i/2)(1 + t)/2, t^2, t^2(1 + i/2)\}$ and $\theta = \{\pi/10, 3\pi/10, \pi/2\}$.

In Figures 6(a)–6(c), the reflection coefficient $|R|$ is plotted against wave numbers Ku for DW, for $v/u = 0.1$, the porosity parameter $\lambda(t) = \{1, 1 + i/2, (1 + t)/2, (1 + i/2)(1 + t)/2, t^2, t^2(1 + i/2)\}$ and $\theta = \{\pi/10, 3\pi/10, \pi/2\}$.

https://doi.org/10.1017/S1446181124000221 Published online by Cambridge University Press

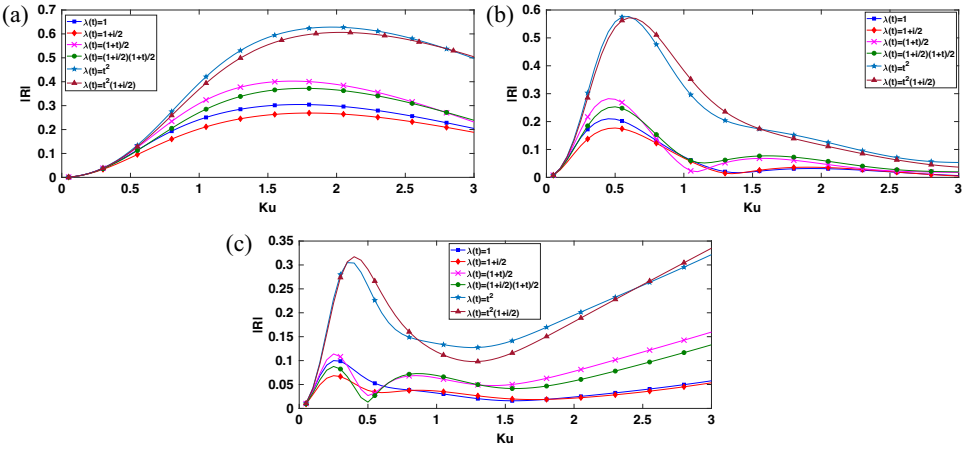

FIGURE 6. $|R|$ against Ku for $v/u = 0.1$, (a) $\theta = \pi/10$, (b) $\theta = 3\pi/10$, (c) $\theta = \pi/2$.

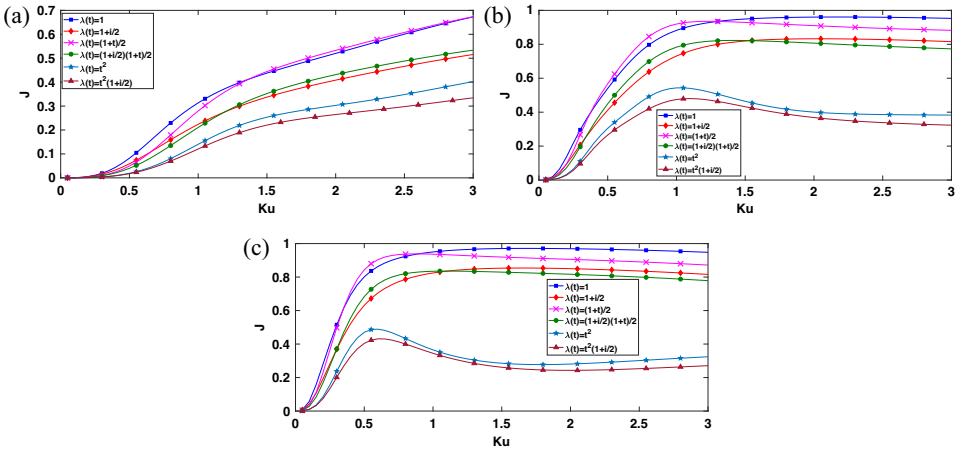

FIGURE 7. J against Ku for $v/u = 0.1$: (a) $\theta = \pi/10$; (b) $\theta = 3\pi/10$; (c) $\theta = \pi/2$.

It is observed from Figures 6(a)–6(c) that for each $\theta = \{\pi/10, 3\pi/10, \pi/2\}$,

$$|R|_{\lambda(t)=t^2} > |R|_{\lambda(t)=(1+t)/2} > |R|_{\lambda(t)=1}, \quad |R|_{\lambda(t)=t^2(1+i/2)} > |R|_{\lambda(t)=(1+t)(1+i/2)/2} > |R|_{\lambda(t)=1+i/2}$$

for $-1 < t < 1$ in general. This shows that a barrier with these particular choices of nonuniform porosity induces more reflection than that of a barrier with constant porosity.

https://doi.org/10.1017/S1446181124000221 Published online by Cambridge University Press

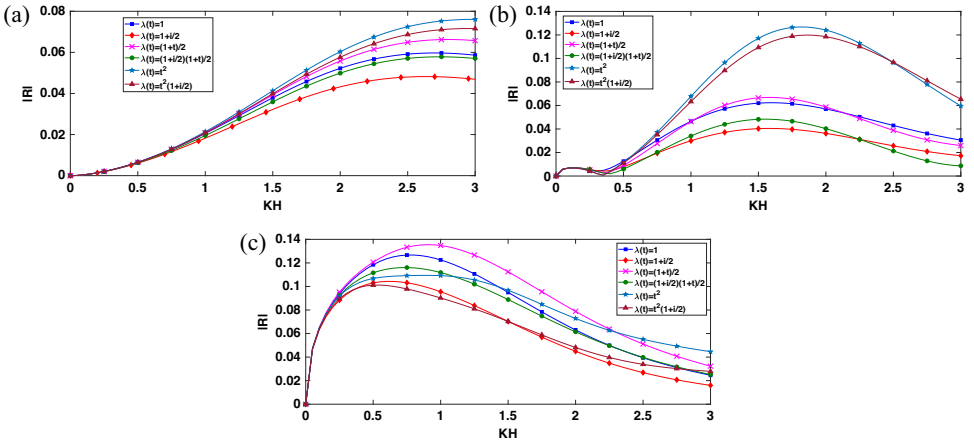

FIGURE 8. $|R|$ against KH for $v/H = 0.3$, $u/H = 0.5$, for (a) $\theta = \pi/10$, (b) $\theta = 3\pi/10$, (c) $\theta = \pi/2$.

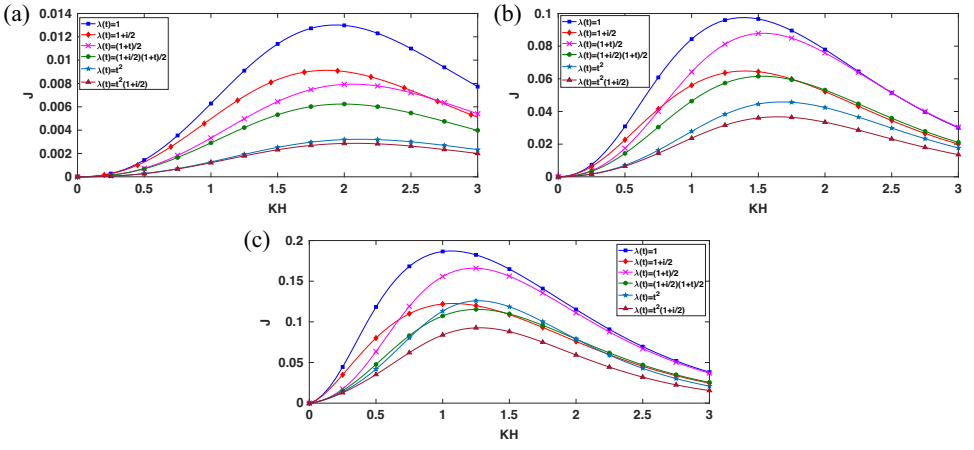

FIGURE 9. J against KH for $v/H = 0.3$, $u/H = 0.5$, for (a) $\theta = \pi/10$, (b) $\theta = 3\pi/10$, (c) $\theta = \pi/2$.

In Figures 7(a)–7(c), the amount of wave energy dissipated J is plotted against wave numbers Ku for DW, for $v/u = 0.1$, the porosity parameter $\lambda(t) = \{1, 1 + i/2, (1 + t)/2, (1 + i/2)(1 + t)/2, t^2, t^2(1 + i/2)\}$ and $\theta = \{\pi/10, 3\pi/10, \pi/2\}$. From Figures 7(a)–7(c), the following observations are made.

(i) For a short barrier, $\theta = \pi/10$, $J_{\lambda(t)=(1+t)/2} > J_{\lambda(t)=1}$ for $Ku > 1.4$. This shows that a nonuniform porous barrier whose porosity increases circumferentially from one end to the other end dissipates energy of short crested surface waves more than for a barrier with a uniform porosity distribution. This confirms the efficacy of a nonuniform

https://doi.org/10.1017/S1446181124000221 Published online by Cambridge University Press

porous barrier with this particular porosity distribution over a uniform porous barrier as a model for breakwater. As the length of the barrier increases, the energy dissipation for short-crested waves is more for a barrier with uniform porosity than for a barrier with nonuniform porosity.

(ii) For any length of the barrier, the energy dissipation coefficient J for a barrier which is rigid at the centre and porous towards the end is least.

(iii) $J_{\lambda_{\text{real}}} > J_{\lambda_{\text{complex}}}$ showing that the inertial force coefficient of the porous barrier allows the passage of water through the pores of the barrier and thereby prevents dissipation of wave energy.

Behaviour of $|R|$ and J for water of finite depth. In Figures 8(a)–8(c), the reflection coefficient $|R|$ for FDW is plotted against the wave number KH, for $v/H = 0.3$, $u/H = 0.5$, the porosity parameter $\lambda(t) = \{1, 1 + i/2, (1 + t)/2, (1 + i/2)(1 + t)/2, t^2, t^2(1 + i/2)\}$ and $\theta = \{\pi/10, 3\pi/10, \pi/2\}$.

From these figures, we make the following observations.

(1) From Figures 8(a)–8(c), it is observed in general that $|R|_{\lambda_r} > |R|_{\lambda_r + i\lambda_i}$ for all values of $\lambda(t) = \{1, 1 + i/2, (1 + t)/2, (1 + i/2)(1 + t)/2, t^2, t^2(1 + i/2)\}$, which shows that the presence of an inertial force coefficient in the porous barrier allows the passage of water through it and thereby reduces the reflection.

(2) Figure 8(a) shows that for $KH > 1$,

$$|R|_{\lambda(t)=t^2} > |R|_{\lambda(t)=(1+t)/2} > |R|_{\lambda(t)=1}, \quad |R|_{\lambda(t)=t^2(1+i/2)} > |R|_{\lambda(t)=(1+i/2)(1+t)/2} > |R|_{\lambda(t)=(1+i/2)},$$

which infers that for a small arc length of the barrier ($\theta = \pi/10,\ 3\pi/10$), the reflection of waves with moderate to short wavelength is more for the barrier which is rigid at the centre and porous towards the ends ($\lambda(t) = t^2,\ t^2(1 + i/2)$) than for the barrier which is rigid at one end and becomes porous towards the other end ($\lambda(t) = (1 + t)/2$, $(1 + i/2)(1 + t)/2$). Moreover, the reflection coefficient for these waves for a barrier with constant porosity is less than the barrier with variable porosity. Also for $KH < 1$, that is, the long waves which are towards the bottom, they do not feel the presence of the barrier. Almost similar behaviour is observed from Figure 8(b) when $\theta = 3\pi/10$. It may be mentioned that for $KH > 2.2$, $|R|_{\lambda(t)=1} > |R|_{\lambda(t)=(1+t)/2}$.

However, when the length of the barrier increases to $\pi/2$, the change in the behaviour of $|R|$ can be observed from Figure 8(c). For $KH < 0.3$, $|R|$ coincides for all values of $\lambda(t)$ showing that the long waves do not feel the presence of the barrier. For $0.3 < KH < 1.5$, $|R|_{\lambda(t)=(1+t)/2} > |R|_{\lambda(t)=1} > |R|_{\lambda(t)=t^2}$. For $1.5 < KH < 2.3$, $|R|_{\lambda(t)=(1+t)/2} > |R|_{\lambda(t)=t^2} > |R|_{\lambda(t)=1}$ and for $KH > 2.3$, $|R|_{\lambda(t)=t^2} > |R|_{\lambda(t)=(1+t)/2} > |R|_{\lambda(t)=1}$. Almost similar behaviour in $|R|$ is observed when the inertial force coefficient is present in the porous material of the barrier.

Thus, for these choices of porosity distributions of the barrier, the behaviour of $|R|$ in the case of finite depth of water region (FDW) is different from the behaviour of $|R|$ for deep water (DW), which may be attributed to the interaction of waves with the porous barrier and the bottom of the water region.

Figures 9(a)–9(c) capture the behaviour of wave energy dissipation coefficient J for FDW for various values of the wave number KH, depth of the barrier below the

https://doi.org/10.1017/S1446181124000221 Published online by Cambridge University Press

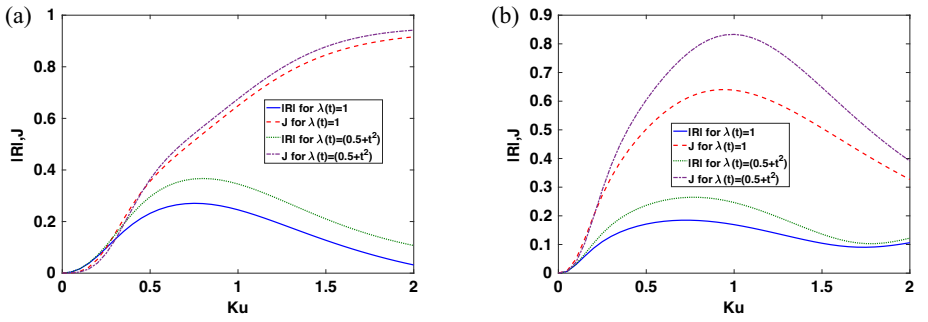

FIGURE 10. (a) $|R|$ and J against Ku for $v/u = 0.1$, $\theta = \pi/5$ for deep water, (b) $|R|$ and J against Ku for $v/u = 0.1$, $H/u = 1.2\theta = \pi/5$ for water of finite depth.

mean free surface, that is, $v/H = 0.3$, radius of the barrier, that is, $u/H = 0.5$, and the porosity parameter $\lambda(t) = \{1, 1 + i/2, (1 + t)/2, (1 + i/2)(1 + t)/2, t^2, t^2(1 + i/2)\}$ and $\theta = \{\pi/10, 3\pi/10, \pi/2\}$.

(1) It is observed from these figures that

$$J_{\lambda(t)=t^2} < J_{\lambda(t)=(1+t)/2} < J_{\lambda(t)=1},$$
$$J_{\lambda(t)=t^2(1+i/2)} < J_{\lambda(t)=(1+t)(1+i/2)/2} \leq J_{\lambda(t)=1+i/2},\ -1 < t < 1$$

for $\theta = \{\pi/10, 3\pi/10, \pi/2\}$. This shows that energy dissipation for a barrier with constant porosity is more than that of a barrier with variable porosity. Also the energy dissipation is least for $\lambda(t) = t^2,\ t^2(1 + i/2)$.

(2) From these figures, it is seen that for a particular value of KH, J increases as θ increases. This shows that the dissipation of wave energy increases with length of the curved barrier.

(3) Also from these figures, $J_{\lambda_r} > J_{\lambda_r + i\lambda_i}$ for any length of the barrier. So the inertial force coefficient of the porous barrier increases transmission and prevents dissipation of the wave energy.

Comparison of uniform and nonuniform porosity distribution. Figure 10(a) depicts $|R|$ and J against Ku for $v/u = 0.1, \theta = \pi/5$ for deep water while Figure 10(b) depicts $|R|$ and J against Ku for $v/u = 0.1, H/u = 1.2\theta = \pi/5$ for water of finite depth for uniform porosity distribution given by $\lambda(t) = 1$ and for nonuniform porosity distribution $\lambda(t) = (0.5 + t^2)$. This particular choice of nonuniform porosity distribution shows that the porosity is less near the middle of the barrier and increases towards the ends of the barrier. From both figures, it is seen that energy dissipation J for nonuniform porosity is more than that of uniform porosity. In particular, the J for a barrier with nonuniform porosity is significantly more than J for a barrier with uniform porosity when the water is of finite depth. This shows that a barrier with porosity distribution $\lambda(t) = (0.5 + t^2)$ reduces the wave power by dissipating the energy, and thus serves as a better model for breakwater than a barrier with uniform porosity. This phenomenon is also observed in Figure 7(a).

https://doi.org/10.1017/S1446181124000221 Published online by Cambridge University Press

5. Conclusion

The present work is concerned with a study of the phenomenon of scattering of incident waves by a porous curve barrier in water with finite and infinite depth. The problem is formulated in terms of a hypersingular integral equation of second kind where the unknown function represents the difference of potentials across the curve barrier. The integral equation is then solved by two methods, namely, the boundary element method and the collocation method. Using the solution of the integral equation, the reflection coefficient and the amount of wave energy dissipated are obtained which are depicted graphically against the wave number choosing different types of porosity distributions in the barrier. An important observation from the graphical representation is that for a certain choice of nonuniform porosity distribution in the barrier, the energy dissipation can be enhanced and thereby the wave power can be reduced, making the barrier a better model for breakwater.

The behaviour of reflected waves and the energy dissipation coefficient in the case of finite depth of the water region is somewhat different from the behaviour of the same for deep water and may be attributed to the interaction of waves with the porous barrier and the bottom of the water region.

Acknowledgement

This work is partially supported by the State Government Departmental Fellowship, Government of West Bengal.

References

[1] S. Banerjee, D. Mondal and S. Banerjea, "Wave response to a nonuniform porous vertical plate", *J. Mar. Sci. Applcs.* (2024); doi:10.1007/s11804-024-00543-x.

[2] J. Dai, C. M. Wang, T. Utsunomiya and W. Duan, "Review of recent research and developments on floating breakwaters", *Ocean Eng.* **158** (2018) 132–151; doi:10.1016/j.oceaneng.2018.03.083.

[3] S. Gupta and R. Gayen, "Water wave interaction with dual asymmetric non-uniform permeable plates using integral equations", *Appl. Math. Comput.* **346** (2019) 436–451; doi:10.1016/j.amc.2018.10.062.

[4] M. Kanoria and B. N. Mandal, "Water wave scattering by a submerged circular-arc-shaped plate", *Fluid Dyn. Res.* **31** (2002) Article ID: 317; doi:10.1016/S0169-5983(02)00136-3.

[5] Y. Liu and H. J. Li, "Analysis of wave interaction with submerged perforated semi-circular breakwaters through multipole method", *Appl. Ocean Res.* **34** (2012) 164–172; doi:10.1016/j.apor.2011.08.003.

[6] B. N. Mandal and A. Chakrabarti, *Water wave scattering by barriers*, 4th edn (WIT Press, Southampton, UK, 2000); https://api.semanticscholar.org/CorpusID:92876695.

[7] M. McIver and U. Urka, "Wave scattering by circular arc shaped plates", *J. Engrg. Math.* **29** (1995) 575–589; doi:10.1007/BF00044123.

[8] A. Mondal, S. Panda and R. Gayen, "Flexural-gravity wave scattering by a circular-arc-shaped porous plate", *Stud. Appl. Math.* **138** (2017) 77–102; doi:10.1111/sapm.12137.

[9] D. Mondal and S. Banerjea, "Scattering of water waves by a porous circular arc-shaped barrier submerged in ocean", *Int. J. Comput. Methods Exp. Meas.* **4** (2016) 532–542; doi:10.2495/cmem-v4-n4-532-542.

[10] D. Mondal, S. Banerjee and S. Banerjea, "Effect of thin vertical porous barrier with variable permeability on an obliquely incident wave train", *Wave Motion* **126** (2024) Article ID: 103262; doi:10.1016/j.wavemoti.2023.103262.

[11] D. Mondal, A. Samanta and S. Banerjea, "Hypersingular integral equation formulation of the problem of water wave scattering by a circular arc shaped impermeable barrier submerged in water of finite depth", *Quart. J. Mech. Appl. Math.* **74** (2021) 491–505; doi:10.1093/qjmam/hbab012.

[12] N. F. Parsons and P. A. Martin, "Scattering of water waves by submerged curved plates and by surface-piercing flat plates", *Appl. Ocean Res.* **16** (1994) 129–139; doi:10.1016/0141-1187(94)90024-8.

[13] A. Samanta, R. Chakraborty and S. Banerjea, "Line element method of solving singular integral equations", *Indian J. Pure Appl. Math.* **53** (2022) 528–541; doi:10.1007/s13226-021-00115-7.

[14] A. Samanta, D. Mondal and S. Banerjea, "Water wave interaction with a circular arc shaped porous barrier submerged in a water of finite depth", *J. Engrg. Math.* **138** (2023) 4; doi:10.1007/s10665-022-10248-1.

[15] B. Sarkar, S. De and R. Roy, "Obliquewave scattering by two thin non-uniformpermeable vertical walls with unequal apertures in water of uniform finite depth", *Waves Random Complex Media* **31** (2021) 2021–2039; doi:10.1080/17455030.2020.1716106.

[16] M. Singh, R. Gayen and S. Kundu, "Linear water wave propagation in the presence of an inclined flexible plate with variable porosity", *Arch. Appl. Mech.* **92** (2022) 2593–2615; doi:10.1007/s00419-022-02201-6.

[17] S. M. Sobhani, J. J. Lee and L. C. Wellford Jr, "Interaction of periodic waves with inclined portable barrier", *J. Waterway Port Coastal Ocean Eng.* **114** (1988) 745–761; doi:10.1061/(ASCE)0733-950X(1988)114:6(745).

[18] H. Song and L. Tao, "An efficient scaled boundary FEM model for wave interaction with a nonuniform porous cylinder", *Internat. J. Numer. Methods Fluids* **63** (2010) 96–118; doi:10.1002/fld.2080.

[19] L. Tao, H. Song and S. Chakrabarti, "Wave interaction with a perforated circular breakwater of non-uniform porosity", *J. Engrg. Math.* **65** (2009) 257–271; doi:10.1007/s10665-009-9287-x.

[20] X. Yu, "Diffraction of water waves by porous breakwaters", *J. Waterway Port Coastal Ocean Eng.* **121** (1995) 275–282; doi:10.1061/(ASCE)0733-950X(1995)121:6(275).